Atmos. Chem. Phys., 24, 9309–9322, 2024
https://doi.org/10.5194/acp-24-9309-2024

Atmospheric Chemistry and Physics
Open Access
EGU

Research article

Mechanistic insight into the kinetic fragmentation of norpinonic acid in the gas phase: an experimental and density functional theory (DFT) study

Izabela Kurzydym[1,3], Agata Błaziak[2], Kinga Podgórniak[1,3], Karol Kułacz[1,3], and Kacper Błaziak[1,3]

[1]Faculty of Chemistry, University of Warsaw, ul. Pasteura 1, 01-224 Warsaw, Poland
[2]Institute of Physical Chemistry, Polish Academy of Sciences, Warsaw 01-224, Poland
[3]Biological and Chemical Research Centre, University of Warsaw, ul. Żwirki i Wigury 101, 01-224 Warsaw, Poland

Correspondence: Kacper Błaziak (kblaziak@chem.uw.edu.pl)

Received: 6 March 2024 – Discussion started: 7 March 2024
Revised: 14 June 2024 – Accepted: 30 June 2024 – Published: 27 August 2024

Abstract. Norpinonic acid has been known as an important α-pinene atmospheric secondary organic aerosol (SOA) component. It is formed in the reaction of α-pinene, β-pinene or verbenone with atmospheric oxidizing reagents. In the presented study, tandem mass spectrometry techniques were used to determine the exact norpinonic acid fragmentation pathway in the gas phase. The precursor anion – deprotonated norpinonic acid (m/z 169), generated in an electrospray (ESI) source – was introduced into the collision cell of the mass spectrometer and fragmented using the energy-resolved collision-induced dissociation (ER-CID) technique. The experimental energy values of degradation processes were determined via analysis of the breakdown curves. Quantum chemical calculations of the reaction models were also constructed, including calculation of all transition states. Comparison between the experimental and the theoretical threshold energies calculated at a ωB97XD/6-311+G(2d,p) theoretical level has shown a good correlation. Two basic pathways of the fragmentation of the parent anion $[M\text{-}H]^-$ (m/z 169) were observed. Firstly this leads to the decarboxylation product (m/z 125) and secondly to the loss of a neutral molecule (C_4H_6O), together with the formation of the anion m/z 99. On the other hand, the breakdown of the anion m/z 125 gives rise to the m/z 69, 57 and 55 ions. To confirm structures formed during ER-CID experiments, the gas-phase proton transfer reactions were examined of all norpinonic acid anionic fragments with a series of neutral reagents, characterized by proton affinity (PA) values. Based on PA difference analysis, the most possible chemical structures were proposed for the observed fragment anions.

1 Introduction

Earth's atmosphere contains a tremendous number of organic compounds, which differ in fundamental properties, such as volatility, reactivity, hygroscopicity and propensity to form cloud droplets (Hallquist et al., 2009). It is estimated that 10 000 to 100 000 different organic compounds have been measured in the atmosphere (Goldstein, 2007). Primary organic aerosols are emitted to the atmosphere directly from a wide variety of natural and anthropogenic sources (Hallquist et al., 2009). Globally, about 1300 Tg of volatile organic compounds (VOCs) is emitted each year to the atmosphere, from biomass burning, combustion of fossil fuels, volcanic eruptions and vegetation processes (Seinfeld and Pandis, 2016; Olsson and Benner, 1999). The chemical reactions of VOCs with different atmospheric oxidizing reagents, such as ozone (O_3), OH radicals and NO_3 radicals, result in secondary organic aerosol (SOA) formation (Gómez-González et al., 2012; George and Abbatt, 2010; Kavouras et al., 1999).

Studies on the chemical composition of SOA have reported the formation of a number of multifunctional products, among which a large number of compounds contain carboxylic functional groups. Due to their low volatility, mono-,

di- and tricarboxylic acids have been also suggested as key species in gas-to-particle conversion processes (Claeys et al., 2007; E. Jenkin et al., 2000; Glasius et al., 2000; Christoffersen et al., 1998). Norpinonic acid is considered a semi-volatile organic compound (SVOC) with a vapor pressure of about 1.28×10^{-4} Torr, making it a slightly more significant contributor to the gas-phase air chemical composition than pinic, pinonic or norpinonic acids. Considering this, the potential gas–particle-phase transition of norpinonic acid suggests that its kinetic transformations in the gas phase may play an important role in atmosphere evolution (Ruff, 2018).

Field studies have shown that a few organic acids formed during the α-pinene oxidation process, such as pinic acid, pinonic acid, norpinic acid, norpinonic acid and their isomers, which are prominent components of atmospheric aerosol natural samples (Feltracco et al., 2018; Lignell et al., 2013; Kavouras et al., 1998).

The analytical toolbox available for chemists to study atmospheric organic components has expanded considerably during the past decades (Hallquist et al., 2009). A wide variety of analytical techniques are used for the structural characterization of organic aerosol (OA) products, e.g., gas chromatography–mass spectrometry (GC–MS) (Shao et al., 2022; Tajuelo et al., 2022), liquid chromatography–mass spectrometry (LC–MS) (Resch et al., 2023; Sarang et al., 2023), nuclear magnetic resonance (NMR) (McAlister et al., 2021; Rodriguez et al., 2022) and Fourier transform infrared (FTIR) spectroscopy (Yu et al., 2021; Zanca et al., 2017; Takahama et al., 2016; Finessi et al., 2012). In particular, liquid chromatography in combination with high-resolution negative-ion electrospray ionization mass spectrometry is widely used to identify and quantify the atmospheric aerosol polar and organic compounds (Gómez-González et al., 2012). Identification is mostly based on second-order mass spectra (MS/MS), which together with an elemental composition of target ion signals obtained from high-resolution measurements helps with the structural characterization of the organic compounds (Claeys et al., 2009; Kourtchev et al., 2008; Szmigielski et al., 2007). However, for the proper identification of OA components, mentioned MS/MS measurements should be made very accurately in order to have full confidence in the organic compound structural characterization during the ambient-sample analytical process (Hocart, 2010).

In this publication, we have focused on one of the α-pinene SOA components – norpinonic acid – which is formed in the reaction of α-pinene with atmospheric oxidizing reagents, such as O_3 or OH radicals (Zhang et al., 2015; Ma et al., 2008, 2007; Winterhalter et al., 2003; Peeters et al., 2001). Norpinonic acid is considerably significant, which is about 0.2–1.1 ng m^{-3} (Li et al., 2013). It is known that the majority of the chemical process in the atmosphere are induced by the radical species at both night- and daytime. However, it is also proposed that some of the chemical transformations in the atmosphere may proceed via other chemical routes that do not require the presence of radicals, which might go through anionic or cationic pathways, e.g., the ion cluster formation or deprotonation of acidic structures by basic inorganic agents (Jarrold, 2023; Richards et al., 2020; Hirsikko et al., 2011; Blanco-Heras et al., 2008; Krivácsy et al., 1997; McCrumb and Arnold, 1981). Nevertheless, there are no models proposing intra- or bimolecular reaction paths, e.g., the kinetic or thermodynamic energy-induced degradation process that can break SOA or other organic and inorganic components into fragments within ionic chemical transformations. Organic acids containing one or more carboxylic groups are significant contributors to the total SOA mass, and the norpinonic acid is chosen as a prominent example to rationalize its fragmentation process.

Herein, we studied the norpinonic acid anionic fragmentation pathway in the gas phase and identified the exact ion fragment structures based on the second-order mass spectrum (MS/MS) recorded during energy-resolved collision-induced dissociation (ER-CID) mass spectrometry experiments. Detailed analysis of recorded breakdown curves has been provided, leading to the experimental energy values required for gas-phase degradation processes. In addition, structural analysis has been performed through the bimolecular reactions of norpinonic acid anion and its anionic fragments with a series of neutral reagents (CH_3SCN, CH_3SSCH_3, $CHCl_3$, $CHBr_3$, CH_2Cl_2, CH_3NO_2) to investigate the difference in proton affinity (PA) values based on the observation of the proton transfer reaction. Quantum chemical calculations of the reaction models for all observed fragmentation processes were also conducted, including determination of all transition states presented in the reaction mechanism. Improved knowledge of the structures formed during ER-CID-MS experiments leads to a better understanding of potential atmospheric reaction pathways (Nozière et al., 2015).

2 Experimental section

2.1 General materials and methods

Cis-norpinonic acid was synthesized in the Laboratory of the Environmental Chemistry in the Institute of Physical Chemistry, Polish Academy of Sciences, using an optimized synthetic procedure based on a method previously reported by Moglioni et al. (Moglioni et al., 2000). A detailed synthetic procedure for the preparation and purification of the norpinonic acid along with the IR, ESI-HR-MS (high resolution), and ^{1}H and ^{13}C NMR analytical spectra of the final product are provided in the Supplement (Sect. S1, "Synthesis of investigated compound").

2.2 Mass spectrometry experiments

All experiments were performed using a modified Micromass Waters Q-ToF 2 (time-of-flight) spectrometer (Blaziak

et al., 2018; Błaziak et al., 2017; Miller et al., 2014) equipped with an electrospray (ESI) ion source operated in the negative-ion mode. The norpinonic acid anion (m/z 169) (International Union of Pure and Applied Chemistry, 2019) was generated by introducing to the ESI source an aqueous–methanolic (2 : 1) solution of 1 mM norpinonic acid using a syringe pump at a flow rate of 0.2 mL min^{-1}. The main fragmentation product ions investigated in this work were formed in two ways: upon collision activation in the collision cell by varying the collision kinetic ion energy and in the ion source by varying the capillary and cone voltages accelerating the in-source bond breaking process. For the ER-CID experiments argon (Ar) was used as collision gas, while for the bimolecular gas-phase reactions different reagent vapors were introduced to the collision cell using an in-house gas inlet system (Blaziak et al., 2018; Błaziak et al., 2017; Miller et al., 2014). The bimolecular reactions together with proton affinity analyses were carried out to identify the isomeric and conformational diversity of the norpinonic acid anionic fragments formed in both the collision cell and the ion source of the mass spectrometer. Volatile reagents introduced to the collision cell and used for the bimolecular reactions as neutral reagents were as follows: methyl thiocyanate, dimethyl disulfide, chloroform, bromoform, dichloromethane and nitromethane. In the present study a full series of the breakdown curves was recorded to determine the onset/threshold energies of the norpinonic acid fragmentation reactions. Collision spectra were recorded by varying the collision energy in incremental steps with an energy resolution of 8–25 eV in the lab frame and 5–10 min of collection time at each step. To enable the comparison of the observed process, a linear fit of the approximately linearly rising section of the breakdown curve was performed for each dataset (please see Sect. S3.2 in the Supplement). The onset energy has been defined at each gas pressure by calculation of the energy (x value) at zero intensity ($y = 0$). Additionally, to compare the experimental and theoretical energy landscapes, the gas pressure linear extrapolation was also performed. The onset energies defined at five different gas pressures were similarly linearly extrapolated to the zero pressure point, giving the final threshold energies reported in this work.

2.3 Quantum chemical calculation

All calculations were performed with the Gaussian 09 suite of programs (Frisch et al., 2016). The Cartesian coordinates of the initial geometries were created using the GaussView 5.0 program (Dennington et al., 2009). The geometries of the reactants, products, intermediates and transition states were optimized using the CAM-B3LYP, PBE1PBE and ωB97XD functionals with the same 6-311+G(2d,p) basis set. For more detail about the program and functionals, see the Supplement (Sect. S4). No symmetry restrictions were used during the calculation. Harmonic frequencies were used to identify the ground state structures with all real frequencies and transition states (TSs) with only one imaginary frequency. The IRC (intrinsic reaction coordinate) computations were also performed to ensure that each TS structure corresponds to the desired products and substrates. Zero-point energy (ZPE) corrections were included in energy calculations. A schematic representation of the strategy used to determine the functional that gives the results that most closely approximate the experimental data is presented in Fig. S62 in the Supplement.

3 Results and discussion

3.1 Fragmentation pathway of a norpinonic acid anion

Introducing a methanolic aqueous solution of the norpinonic acid to the electrospray ion source of the mass spectrometer gives a rise to deprotonated anion corresponding to $C_9H_{13}O_3^-$ (m/z 169) in the negative-ion mode. Subjecting these ions to collisional activation leads to the formation of fragment ions, corresponding to $C_8H_{13}O^-$ (m/z 125), $C_5H_7O_2^-$ (m/z 99), $C_3H_5O^-$ (m/z 57), $C_4H_5O^-$ (m/z 69), $C_4H_7^-$ (m/z 55) and C_2HO^- (m/z 41) anions. Representative ER-CID mass spectra of $C_9H_{13}O_3^-$ (m/z 169) as well as for fragment ions (m/z 125 and m/z 99) taken at a center-of-mass collision energy (ECM) of 3.8, 4.1 and 4.3 eV (CM), respectively, with argon collision gas at nominal pressures of 3.54×10^{-4} mbar are shown in Fig. 1.

Additionally, to analyze the energetic requirements for each observed fragmentation pathway, the full set of breakdown curves for all of the ions have been recorded, by varying in a stepwise manner the kinetic collision energy in five different collision gas pressures. The threshold energies were estimated by employing a simple extrapolation procedure, which in detail has been described in the Supplement (Figs. S8–S11, S13–S16, S21–S24, S26–S29, S31–S34, S39–S42 and S44–S47). Figure 2 shows the representative breakdown diagrams of m/z 169, m/z 125 and m/z 99 recorded with Ar collision gas at a nominal pressure of 1.06×10^{-4}, 1.08×10^{-4} and 1.06×10^{-4} mbar, respectively. For other spectra, as well as for additional breakdown curves, please consult the Supplement (Figs. S1–S6, S17–S19 and S35–S37).

The experimentally measured reaction energies and the general fragmentation network of the main m/z 169 norpinonic acid anion has been shown in Fig. 3.

It was found that the parent anion $C_9H_{13}O_3^-$ (m/z 169) undergoes two main fragmentation pathways. The first is expressed by the loss of the neutral fragment C_4H_6O (mass of 70), resulting in formation of a $C_5H_7O_2^-$ (m/z 99) anion with an experimentally established appearance energy of 245 ($\pm$ 73) kJ mol^{-1}. The second is a decarboxylation reaction leading to $C_8H_{13}O^-$ (m/z 125) with an onset energy of 237 ($\pm$ 70) kJ mol^{-1}. In order to establish the detailed fragmentation network of the main anion, separate ER-CID experiments were performed for each of the smaller anionic

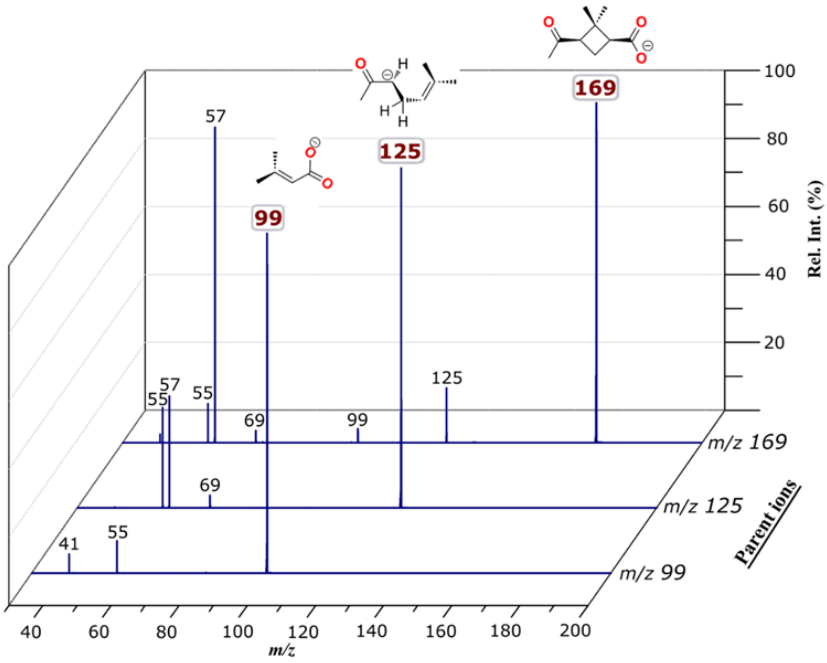

Figure 1. Fragment ion mass spectra of m/z 169, m/z 125 and m/z 99 recorded with a ToF voltage of 3 kV, taken at a collision energy of 3.8, 4.1 and 4.3 eV (ECM), respectively, with argon collision gas at nominal pressures of 3.54×10^{-4} mbar. Rel. Int.: relative intensity.

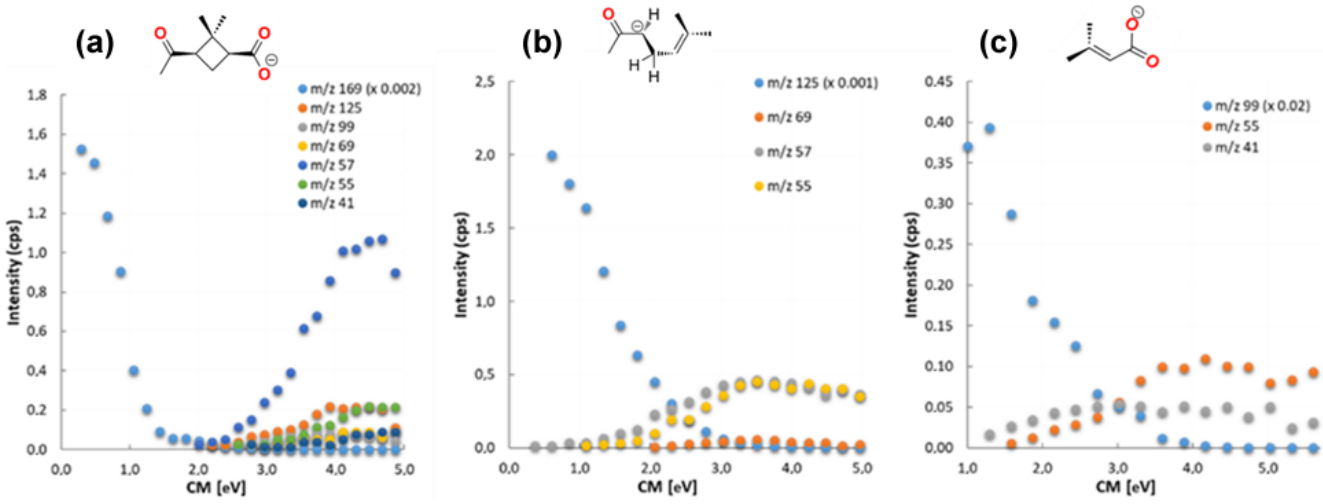

Figure 2. Breakdown curves from the CID experiments on m/z 169 **(a)**, m/z 125 **(b)** and m/z 99 **(c)**, with the ion intensity for the individual ions as a function of ECM. Please note the different scales of the ordinates. The data were recorded with Ar collision gas at a nominal pressure of 1.06×10^{-4}, 1.08×10^{-4} and 1.06×10^{-4} mbar, respectively. cps: counts per second.

fragments that were observed on main-product-ion spectra. Consequently, on the ER-CID mass spectrum of m/z 99, two secondary fragmentation products have been observed: the formation of C_2HO^- (m/z 41) followed by the loss of the neutral molecules of C_3H_6O (see Fig. 5 below), with an estimated fragmentation energy of 72 ($\pm$ 22) kJ mol^{-1}. The anion $C_5H_7O_2^-$ (m/z 99) was also prone to loss of the carbon dioxide molecule (see Fig. 5 below), which leads to the formation of the $C_4H_7^-$ (m/z 55) anion, at the energy of 189 ($\pm$ 57) kJ mol^{-1}. The separate ER-CID experiment for the m/z 125 anion has shown that in-cell activation leads to three different fragmentation pathways. In the first route, the m/z 69 anion is formed by the loss of the neutral molecule C_4H_8 (mass of 56; see Fig. 4 below), with an experimentally established appearance energy of 178 ($\pm$ 53) kJ mol^{-1}. The second pathway leads to the formation of the anionic compound $C_3H_5O^-$ (m/z 57) and the loss off of the neutral molecule C_5H_8 (mass of 68; see Fig. 4 below), with a

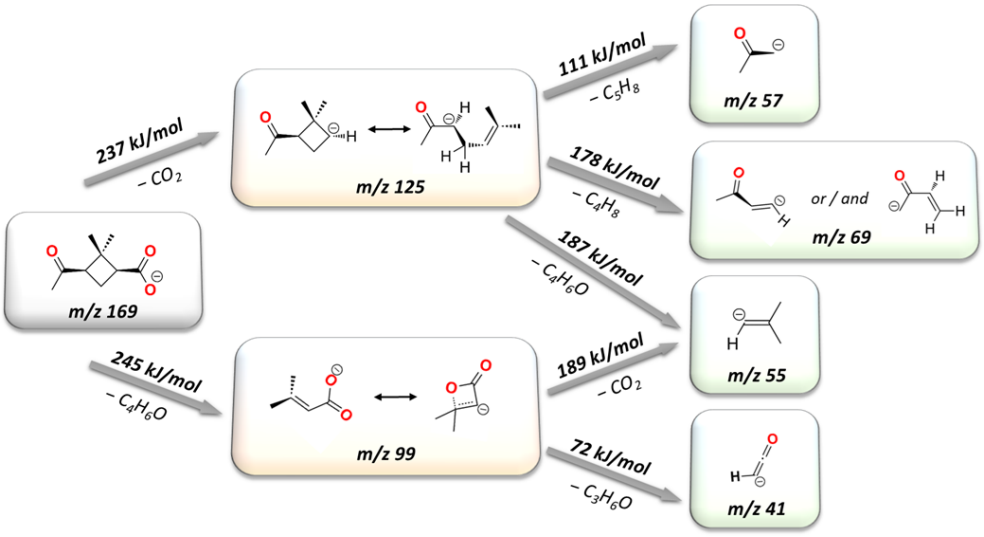

Figure 3. The fragmentation network for deprotonated norpinonic acid (m/z 169). Please note that above the gray arrows the experimental threshold energies (kJ mol^{-1}) for each fragmentation reaction are shown. Below the arrow is the formula of the neutral particle being dropped off.

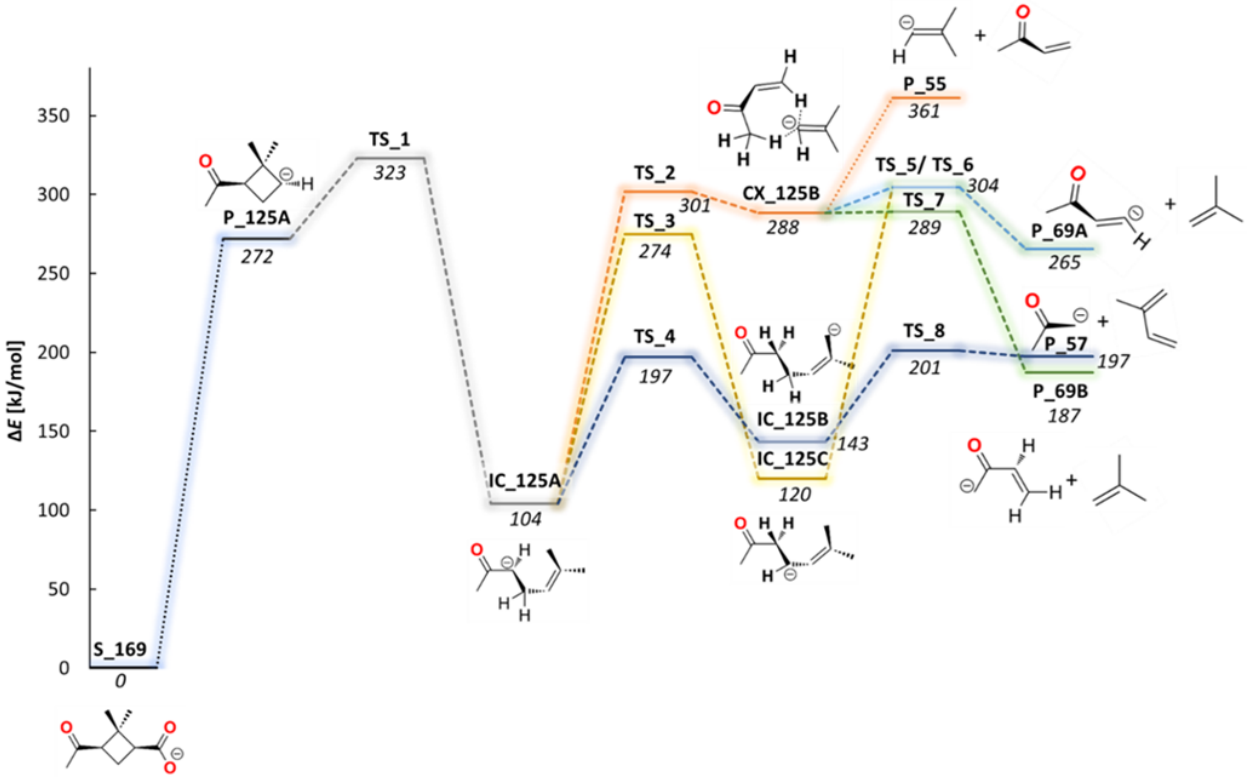

Figure 4. Computed potential energy (ωB97XD/6-311+G(2d,p)) diagrams describing the first fragmentation pathway of m/z 169 ions via m/z 125 to the smaller anionic fragments of m/z 69, m/z 57 and m/z 55. Abbreviations used in the structure names: S for substrate, P for product, TS for transition state, IC for intermediate structure and CX for intermediate complex.

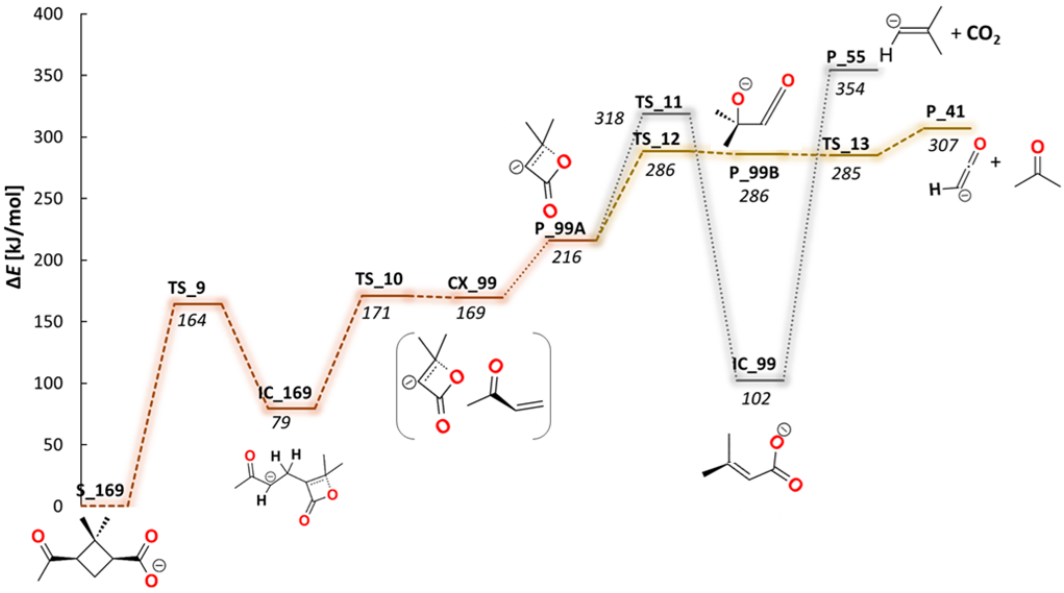

Figure 5. Computed potential energy (ωB97XD/6-311+G(2d,p)) diagrams describing the second fragmentation pathway of m/z 169 ions via m/z 99. Abbreviations used in the structure names: S for substrate, P for product, TS for transition state, IC for intermediate structure and CX for intermediate complex.

determined energy of 111 ($\pm$ 33) kJ mol^{-1}. Finally, a third observed fragmentation pathway gives a rise to the mass signal corresponding to the $C_4H_7^-$ (m/z 55) anion along with the formation of the neutral molecule C_4H_6O (mass of 70). Extrapolation of the linearly rising section of the breakdown curve for m/z 55 gives an onset energy of 187 ($\pm$ 56) kJ mol^{-1} for this process.

3.2 Structural analysis of observed ion fragments

Further insight into the observed fragmentation pathway of deprotonated norpinonic acid (m/z 169) was obtained through quantum chemical calculations. In particular, we applied three different density functional theory (DFT) methods – ωB97XD/6-311+G(2d,p), CAM-B3LYP/6-311+G(2d,p) and PBE1PBE/6-311+G(2d,p) – to explore the energetic and conformational landscape of observed fragmentation processes. In general, all employed methods were found to properly describe the main experimental observations. We have chosen to highlight in the main text the results obtained with the ωB97XD hybrid density functional since this method reproduces the experimental observation most accurately (Chai and Head-Gordon, 2008). The computational method that most closely matched the experimental results was chosen on the basis of the correlation plots of the results. The correlation coefficient for the ωB97XD method was $R^2 = 0.76$ (Fig. 6), while that for the other two was 0.75 and 0.73 (PBE1PBE and B3LYP, respectively; Figs. S63 and S64 in the Supplement). For the comparison with the other theoretical results, please consult the Supplement (Tables S8–S10).

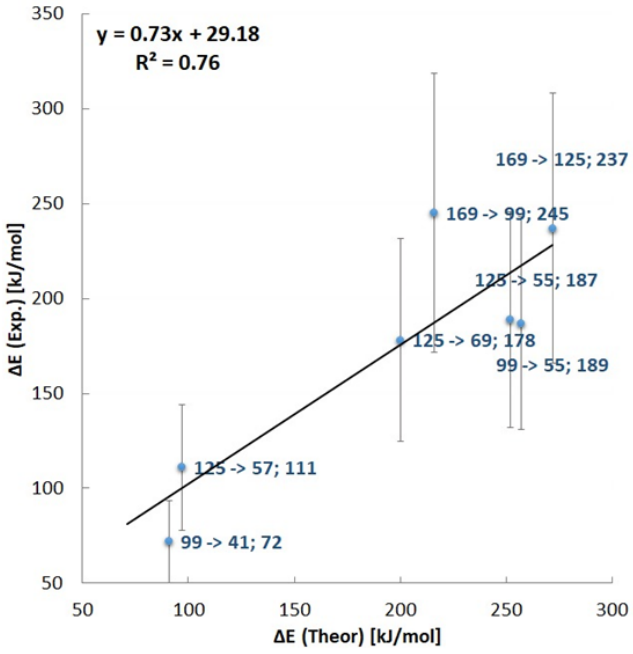

Figure 6. A correlation between experimental and theoretical fragmentation energies obtained with a ωB97XD/6-311+G(2d,p) theoretical level.

Reaction models for all observed fragmentation processes were computationally modeled, including the determination of all possible transition states (TS) and alternative fragmentation pathways that form the full reaction mechanism. The selection of the conformer of norpinonic acid is performed

according to the following procedure: the energies of all possible conformers are optimized, and then statistical analysis is carried out according to the Boltzmann equation to select the conformer occurring in predominance. The potential energy surface for the first main fragmentation pathway leads to the $C_8H_{13}O^-$ (m/z 125) anion formation of other smaller fragments, together with established chemical structures as shown in Fig. 4.

The decarboxylation reaction of the deprotonated norpinonic acid $C_9H_{13}O_3^-$ (m/z 169) leads to the cyclic structure of m/z 125 (P_125A). Further DFT analysis of the fragmentation products of the anion m/z 125 has shown that P_125A is able to be rearranged by the cleavage of a four-membered carbon ring to the more thermodynamically stable "open" structure IC_125A via a relatively low energy barrier TS_1 at 51 kJ mol^{-1} above the P_125A energy level. Interestingly, a similar breaking of a four-member ring had been formally reported earlier by Yasmeen et al. (2010), where the fragmentation of norpinic acid – as a product of the oxidation reaction of norpinonic acid – was discussed. Notably, this observation has a fundamental impact on further mechanistic analysis and for understanding the thermodynamic and kinetic nature of generated ions. The m/z 125 ion is formed in the collision chamber of the mass spectrometer from the precursor ion m/z 169 (during ER-CID experiments). By precisely dosing the ion collision energy, a kinetically controlled product (P_125A) is formed. Due to this fact an excellent correlation between the experimental (237 ($\pm$ 70) kJ mol^{-1}) and computed energies (272 kJ mol^{-1}) for the decarboxylation reaction of m/z 169 ion has been noted. On the other hand, to provide the quantitative energy measurements for subsequent fragmentation reactions of smaller fragments, the initial in-source fragmentation of m/z 169 was performed. Due to thermodynamic conditions of the electrospray ionization and fragmentation processes in the ion source, the in-source formed m/z 125 ions will more likely take the open IC_125A isomeric form. Taking this into account, from this point the thermodynamic open isomer IC_125A is used as a reference for subsequent measurements. In this respect, further collisional activation analysis of in-source formed m/z 125 ions has shown that this anion undergoes three fragmentation pathways. Calculations of the first proposed fragmentation pathway of m/z 125 lead to a m/z 55 anion via one transition state (TS_2) and the intermediate structure CX_125B. It was found that the anion $C_4H_7^-$ (m/z 55) is formed together with the neutral molecule C_4H_6O (mass of 70), which is attributed to the methyl vinyl ketone (MVK) structure (P^o_70), placed 257 kJ mol^{-1} above the IC_125A energy level. The CX_125B intermediate complex can also undergo alternative transformation through a transition state (TS_5) to the anion m/z 69. Transition state energy (TS_5) was calculated to be 200 kJ mol^{-1} above the IC_125A energy level. In this step of the reaction mechanism, the anion m/z 69 (P_69A) is formed, together with the neutral molecule C_4H_8 (mass of 56), which corresponds to a neutral molecule of a 2-methylpropene chemical structure (P^o_56). On the other hand, the alternative mechanism for the m/z 69 anion formation may lead to a P_69B structure through a different transition state (TS_7), which has lower energetic requirements. The energy of TS_7 was calculated at 185 kJ mol^{-1} above the IC_125A energy level. A third calculated pathway leads to the formation of the anionic compound $C_3H_5O^-$ (m/z 57) by the loss of the neutral fragment C_5H_8 (mass of 68) corresponding to a 2-methyl-1,3-butadiene structure, also known as isoprene (P^o_68). It was found that two consecutive transition states lead to the formation of the m/z 57 anion through the IC_125B intermediate, calculated to be 197 kJ mol^{-1} and 201 kJ mol^{-1}, for TS_4 and TS_8, respectively. Notably, the experimental appearance energy for m/z 57 formation estimated from the experiment (111 ($\pm$ 33) kJ mol^{-1}) is slightly higher than the computed transition state energy values (97 kJ mol^{-1}).

The second part of the potential energy diagram calculated for the fragmentation pathway of the main m/z 169 anion that leads through the m/z 99 ion to the formation of the smaller ion fragments m/z 41 and 51 is shown in Fig. 5.

It has been shown that the primary fragmentation product, the m/z 99 anion, can form three alternative isomeric structures, first where the anion is located on the carbon atom (P_99A) or second where negative charge occurs on the oxygen atom (P_99B) and intermediate product (IC_99). The structure P_99A is formed in an exothermic process that formally proceeds through two transition states – TS_9 and TS_10 – and two intermediate mechanistic points – intermediate structure IC_169 and intermediate complex CX_99 – with the ultimate reaction energy for P_99A calculated at 216 kJ mol^{-1}. This part of the mechanism can be referred to as the kinetic ER-CID experimental results with an estimated energy for m/z 99 ion formation of 245 kJ mol^{-1}. Based on the computed chemical transformations of the m/z 99 ion, it is seen that the more thermodynamically stable isomer P_99B can be formed via opening of a lactone ring that is emphasized by the transition state TS_12, located 70 kJ mol^{-1} above the P_99A energy level. It is worth mentioning that further separate ER-CID experiments performed on the m/z 99 anion required its initial in-source generation. In this respect, we think that again here the more thermodynamically stable isomer of the m/z 99 anion of P_99A is formed while generated in the ion source, from which further experimental measurements in the collision cell took place.

The DFT computations show that after the transition state TS_12, the isomer P_99B is formed, from which an exothermic path leads to the formation of the anion m/z 41 by the loss of the neutral molecule C_3H_6O. A fragmentation reaction mechanism has shown that the anion m/z 41 refers to a ketene anion structure. Notably, the experimental appearance energies for the m/z 41 formation reaction estimated from experiments (72 ($\pm$ 22) kJ mol^{-1}) and the computed energy values as an energy difference between P_99A and P_41 (91 kJ mol^{-1}) show a very good correlation. The an-

Table 1. Calculated electron energy values and experimental values (kJ mol^{-1}) for the fragmentation reaction of m/z 169 anions.

	Ion masses	Experimental energy (kJ mol^{-1})	Structure symbols	Theoretical method ωB97XD/6-311+G(2d,p) (kJ mol^{-1})
Fragmentation reaction	169 → 99	245 (± 73)	S_169 → P_99A	216
	99 → 55	189 (± 57)	IC_99 → P_55	252
	99 → 41	72 (± 22)	P_99A→ P_41	91
	169 → 125	237 (± 70)	S_169→P_125A	272
	125 → 69	178 (± 53)	IC_125A→TS_5	200
	125 → 57	111 (± 33)	IC_125A→TS_8	97
	125 → 55	187 (± 56)	IC_125A→P_55	257

ion m/z 55 is generated by a decarboxylation reaction of the anion m/z 99 (IC_99). The energy calculated for this process was found to be 252 kJ mol^{-1}. Calculated energy of the anion m/z 55 formation reaction is slightly higher than the experimental energy estimated with the extrapolation procedure which has been determined as 189 kJ mol^{-1} (Fig. 6, Table 1).

The experimental and the theoretical insight into the fragmentation of the deprotonated norpinonic acid m/z 169 shows that fragmentation through a four-member ring breaking, leading to m/z 99, is a more energetically favorable process than a decarboxylation reaction. It was also reported that the anion m/z 99 forms two possible structures, which differs in the location of the negative charge (P_99A and P_99B) (see Fig. 4). Furthermore, from quantum chemical calculations, the existence of two possible structure were found also for the anion m/z 69 (P_69A and P_69B) as well as for the anion m/z 125 (P_125A and P_125B) (see Fig. 4).

3.3 Proton affinity analysis of anionic fragments

In order to provide more arguments and confirm ion structures formed during ER-CID experiments, we decided to examine the proton transfer reactivity of all formed fragments towards a few different proton donors as neutral reagents, i.e., methyl thiocyanate (CH_3SCN), dimethyl disulfide (CH_3SSCH_3), chloroform ($CHCl_3$), bromoform ($CHBr_3$), dichloromethane (CH_2Cl_2) and nitromethane (CH_3NO_2). The above chemicals have been chosen as a natural representation of species being present in the atmosphere, while their anions provide a wide range of proton affinity (PA) values, giving a chance to investigate a proton transfer reaction with norpinonic acid fragmentation products (Jia et al., 2019; Hossaini et al., 2017; Watts, 2000; Graedel, 2012; Khalil and Rasmussen, 1999; Van Den Berg et al., 1994; Van Den Berg, 1993). The following norpinonic acid anionic fragments were isolated as a result of the in-source generation/fragmentation and subjected into collision cell to perform a bimolecular reaction with neutral species: $C_9H_{13}O_3^-$ (m/z 169), $C_8H_{13}O^-$ (m/z 125), $C_5H_7O_2^-$ (m/z 99), $C_3H_5O^-$ (m/z 57), $C_4H_5O^-$ (m/z 69), $C_4H_7^-$ (m/z 55) and C_2HO^- (m/z 41). Neutral reagents were introduced to the collision cell via an in-house built gas inlet system. For more details about the reaction conditions (vapor pressure of neutral reagents and E_{CM}), please consult the Supplement (Figs. S48–S61). The reactions in the gas phase between neutral reagents and generated anions have shown a number of a new products, which will be described and published in other work in the near future. In this publication, the structural analysis of the generated fragment anions will be performed based on the proton transfer reaction, which relies on differences between the proton affinity values of reacting ions and anionic forms of the vaporous neutral molecules. In Table 2 the results of the observed reactivity of fragment anions with a series of neutral reagents in a proton transfer reaction is briefly summarized.

Proton affinity for each possible fragmentation anion and for the appropriate anions of the involved neutral reagents was computed at a ωB97XD/6-311+G(2d,p) theoretical level and is schematically presented in Fig. S65 in the Supplement and Table 3. For exact proton affinity values calculated at a CAM-B3LYP/6-311+G(2d,p) and PBE1PBE/6-311+G(2d,p) theoretical level, please see the Supplement. Proton affinities calculated for all fragment anions are within the range of 1378 kJ mol^{-1} for deprotonated norpinonic acid (m/z 169) to 1709 kJ mol^{-1} for the anion $C_4H_7^-$ (m/z 55). Computed structures of the anion m/z 69 – P_69A and P_69B (see Fig. 4) – have shown a significant difference in their proton affinity values. For the anion P_69A proton affinity was calculated to be 1611 kJ mol^{-1}, while for the structure P_69B it is 1530 kJ mol^{-1}. The significant difference in proton affinity values was also found for two possible structures calculated for the anion m/z 125. Proton affinity of the structure P_125A was calculated at 1703 kJ mol^{-1}, while for the structure IC_125B it is 1539 kJ mol^{-1}. Proton affinity analysis has shown that the structure P_125A is stronger base than the structure IC_125B. Similar dependence has been also reported for the structure P_69A and P_69B, where the structure P_69A is a stronger base than the structure P_69B. The proton affinity values computed for appropriate anions derived from neutral-reagent proton affini-

Table 2. Proton transfer reaction observed with gas-phase reactions of generated anions with a series of neutral reagents (✓ for reaction observed, – for reaction not observed).

	Proton transfer					
A^-	CH_2Cl_2	$CHBr_3$	$CHCl_3$	CH_3NO_2	CH_3SCN	CH_3SSCH_3
m/z 169	–	–	–	–	–	–
m/z 125	–	✓	✓	✓	–	–
m/z 99	–	✓	✓	✓	–	–
m/z 69	✓	✓	✓	✓	✓	✓
m/z 57	–	✓	✓	✓	–	–
m/z 55	✓	✓	✓	✓	✓	✓
m/z 41	–	✓	✓	✓	–	–

Table 3. Energy of proton affinity of the anionic fragment structures compared with the energy of proton affinities of appropriate deprotonated reagents used in gas-phase reactions obtained by theoretical calculation.

Substrates	Energy of proton affinity ($kJ\,mol^{-1}$)	Anion of neutral reactants	Energy of proton affinity ($kJ\,mol^{-1}$)
P_55	1709	$^-CHCl_2$	1570
P_125A	1703	$CH_3SSCH_2^-$	1550
P_69A	1611	CH_2SCN^-	1549
P_99A	1560	$^-CCl_3$	1501
P_57	1540	$^-CH_2NO_2$	1478
IC_125	1539	$^-CBr_3$	1468
P_69B	1530		
P_41	1527		
P_99B	1434		
S_169	1378		

ties were found to be from 1468 $kJ\,mol^{-1}$ for the bromoform anion to 1570 $kJ\,mol^{-1}$ for the dichloromethane anion. Computed PA values for deprotonated neutral reagents were compared with experimental ones available in the literature and are in good agreement (Afeefy et al., 2011).

The proton transfer reaction with all neutral reagents was observed only for the anions m/z 69 and m/z 55. Dichloromethane was found to react rapidly with the anion m/z 55 in a proton transfer reaction. Similar results were obtained in a reaction with methyl thiocyanate as well as with dimethyl disulfide. The relative intensity of the products for both reagents was low – 2.0 % for the anion m/z 55, 0.1 % for the anion m/z 69 (dimethyl disulfide reaction), 1.8 % for the anion m/z 55 and 0.1 % for the anion m/z 69 (methyl thiocyanate reaction). In the reaction of generated fragments with chloroform, bromoform and nitromethane, we obtained similar/comparable results. The proton transfer reaction was observed for all studied fragments, except the anion m/z 169. The anions m/z 125, m/z 69, m/z 57 and m/z 55 were found to react rapidly with chloroform; the products of the proton transfer reaction were the most abundant. For a reaction towards nitromethane, a high intensity of the proton transfer reaction product was observed for the anions m/z 55 and m/z 57. Mass spectra of the reaction of chloroform, bromoform, dichloromethane and nitromethane towards the anions $C_9H_{13}O_3^-$ (m/z 169), $C_8H_{13}O^-$ (m/z 125), $C_5H_7O_2^-$ (m/z 99), $C_3H_5O^-$ (m/z 57), $C_4H_5O^-$ (m/z 69), $C_4H_7^-$ (m/z 55) and C_2HO^- (m/z 41) together with a relative intensity of the proton transfer reaction product are presented in Fig. 7. For mass spectra of the reaction with methyl thiocyanate as well as with dimethyl disulfide, please consult the Supplement (Figs. S48–S61).

Quantum chemical calculations and gas-phase reactions together with proton affinity analysis turned out to be important to distinguish the structures formed during the collision-induced dissociation (CID) experiments. Quantum chemical calculations have shown two possible structures of the anion m/z 125. However, an analysis of secondary fragmentation products of the anion m/z 125 together with analysis of threshold energies have shown that P_125A is able to rearrange to the more stable structure IC_125A. It appears rational that the anion P_125A is formed in the collision cell during CID experiments of the precursor ion m/z 169 – experimental and theoretical threshold energies showed a good correlation, while, in the ion source, generated anions can rearrange to the more stable linear structure IC_125A. Furthermore, in the gas-phase reaction between the anion m/z 125 and dichloromethane, methyl thiocyanate as well as dimethyl

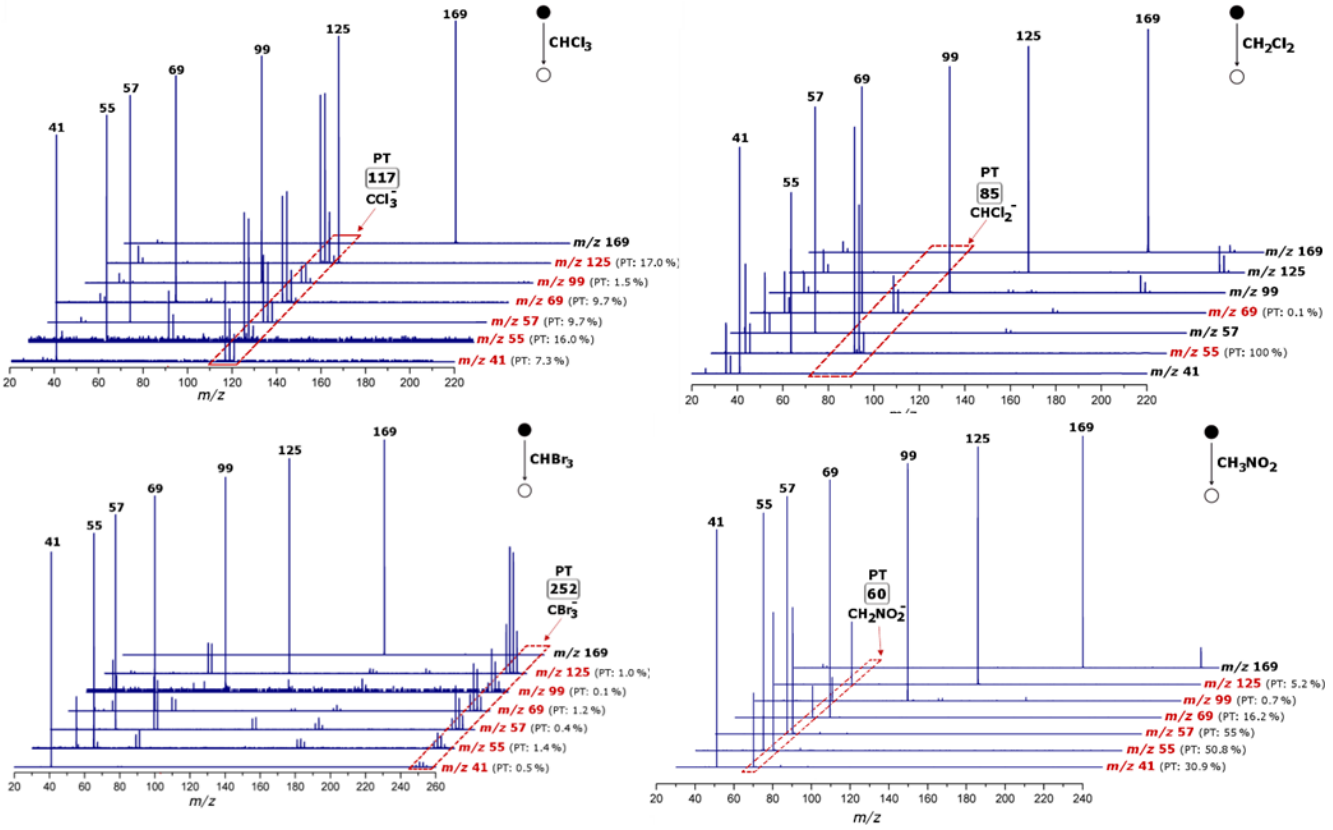

Figure 7. Mass spectra of the reactions between the neutral reagents (chloroform, bromoform, dichloromethane and nitromethane) and the ion-source-generated fragments recorded with a ToF voltage of 3 kV, taken with reagents vapors at nominal pressures of 3.25×10^{-4}, 2.5×10^{-4}, 3.05×10^{-4} and 3.14×10^{-4} mbar, respectively. For the collision energy (ECM) for each anion, please consult the Supplement. PT: proton transfer.

disulfide proton transfer reaction products were not observed. This argument also confirms the hypothesis of the two possible structure of the anion m/z 125, since proton affinity value for P_125A was calculated to be 1703 kJ mol^{-1} (proton transfer reaction product expected), since for the structure IC_125A it was 1558 kJ mol^{-1} (value lower than the proton affinity of dichloromethane, methyl thiocyanate and dimethyl disulfide – a proton transfer reaction should not occur and was not observed). Two possible structures have been also computed for the anion m/z 69. It was found that the anion P_69B need slightly lower energetic requirements to be formed than the anion P_69A, but the difference is not significant so as to unambiguously indicate the structure P_69B as the one. For the anion m/z 69 a small amount of the product of the proton transfer reaction was observed in reaction with all neutral reagents, which clearly proves the presence of P_69A during ER-CID experiments. However, the combination of the lower energetic requirements obtained from quantum chemical computation for the anion P_69B together with a higher proton affinity for P_69A has shown that it is possible for both structures to be generated in ER-CID experiments. In accordance with the computational model, the anion m/z 99 can form two possible structures: one where an anion is located on the carbon atom (P_99A) or another where anion is localized on the oxygen atom (P_99B). The calculated PA value for the structure P_99A is 1557 kJ mol^{-1}, while for P_99B it is 1449 kJ mol^{-1}. The gas-phase reactions of the m/z 99 anion with chloroform, bromoform and nitromethane give rise to a detectable amount of proton transfer reaction products, which clearly indicates the presence of at least some of P_99A structures during ER-CID experiments.

4 Conclusion

The study of the fragmentation pathways of deprotonated norpinonic acid (an important α-pinene oxidation product) was conducted together with structural analysis of the fragments generated during the energy-resolved collision-induced dissociation (ER-CID) experiments. We have shown that quantum chemical calculations and gas-phase reactions supported by proton affinity analysis are reliable methods for the structural analysis of the fragments of deprotonated norpinonic acid (m/z 169).

The breakdown curves for all fragment ions were also measured at variable collision energies and at five different collision gas pressures to estimate the threshold energies, which were measured to be from 72 kJ mol^{-1} for a m/z 41 formation reaction to 245 kJ mol^{-1} for ion m/z 99 formation. Further insight into the observed fragmentation pathway of deprotonated norpinonic acid was obtained through quantum chemical calculations. Comparison between the experimental and the theoretical threshold energies calculated with a ωB97XD/6-311+G(2d,p) theoretical level has shown a good correlation, where the coefficient of determination (R^2) was found to be 0.76. Reaction models for observed fragmentation processes were constructed. Also the minimum energy pathway (MEP) is investigated and presented.

Finally, to distinguish all possible ion structures generated during ER-CID experiments, we examined the reactivity of all fragments towards a series of different neutral reagents – methyl thiocyanate (CH_3SCN), dimethyl disulfide (CH_3SSCH_3), chloroform ($CHCl_3$), bromoform ($CHBr_3$), dichloromethane (CH_2Cl_2) and nitromethane (CH_3NO_2). For structural analysis of generated anions, products of the gas-phase reactions were analyzed for a proton transfer reaction. It was found that the anions m/z 125, m/z 99 and m/z 69 can form two possible structures.

Quantum chemical calculations and the gas-phase reactions together with proton affinity analysis turned out to be a valuable method to reflect the proper structures formed during energy-resolved collision-induced dissociation (ER-CID) experiments. The fragmentation structure proposed for an important α-pinene aging product (norpinonic acid) serves as a useful databank for the atmospheric community and is expected to be extended in the future, for other important aerosol products, including different types of monoterpene SOA.

Data availability. All the experimental and theoretical data sets are available in Supplement.

Supplement. The supplement related to this article is available online at: https://doi.org/10.5194/acp-24-9309-2024-supplement.

Author contributions. IK performed part of the DFT computations and co-wrote the manuscript. AB performed the experiments and DFT computations. KP analyzed part of the experimental breakdown curves. KK co-wrote the manuscript. KB coordinated the project, experiments and theoretical computations and co-wrote the manuscript. All authors have given approval to the final version of the manuscript.

Competing interests. The contact author has declared that none of the authors has any competing interests.

Disclaimer. Publisher's note: Copernicus Publications remains neutral with regard to jurisdictional claims made in the text, published maps, institutional affiliations, or any other geographical representation in this paper. While Copernicus Publications makes every effort to include appropriate place names, the final responsibility lies with the authors.

Acknowledgements. We thank Einar Uggerud and Mauritz Ryding from the University of Oslo, Norway, for their valuable discussions during the project on reaction mechanisms and mass spectrometry experiments. In addition, we express our thanks to the Wrocław Centre for Networking and Supercomputing (WCSS) and Interdisciplinary Centre for Mathematical and Computational Modelling (ICM) in Warsaw (grant no. G50-2) for providing computer time and facilities. We gratefully the acknowledge Polish high-performance computing (HPC) infrastructure PL-Grid (HPC centers: ACK Cyfronet AGH) for providing computer facilities and support (computational grant nos. PLG/2023/016817 and PLG/2023/016626).

Financial support. This research has been supported by the Narodowe Centrum Nauki (OPUS 21, grant no. 2021/41/B/ST10/02748).

Review statement. This paper was edited by Ivan Kourtchev and reviewed by six anonymous referees.

References

Afeefy, H., Liebman, J., and Stein, S.: NIST Chemistry WebBook, NIST Standard Reference Database Number 69, edited by: Linstrom, P. J. and Mallard, W. G., National Institute of Standards and Technology (NIST), https://webbook.nist.gov/chemistry/ (last access: 12 August 2024), 2011.

Blanco-Heras, G. A., Turnes-Carou, M. I., López-Mahía, P., Muniategui-Lorenzo, S., Prada-Rodríguez, D., and Fernández-Fernández, E.: Determination of organic anions in atmospheric aerosol samples by capillary electrophoresis after reversed pre-electrophoresis, Electrophoresis, 29, 1347–1354, https://doi.org/10.1002/elps.200700413, 2008.

Blaziak, K., Tzeli, D., Xantheas, S. S., and Uggerud, E.: The activation of carbon dioxide by first row transition metals (Sc–Zn), Phys. Chem. Chem. Phys., 20, 25495–25505, https://doi.org/10.1039/C8CP04231D, 2018.

Błaziak, K., Miller, G. B. S., Ryding, M. J., and Uggerud, E.: Reaction Model for the Formation of Benzene from Benzoates and Grignard Reagents, Eur. J. Org. Chem., 2017, 4272–4276, https://doi.org/10.1002/ejoc.201700816, 2017.

Chai, J.-D. and Head-Gordon, M.: Long-range corrected hybrid density functionals with damped atom–atom dispersion corrections, Phys. Chem. Chem. Phys., 10, 6615–6620, https://doi.org/10.1039/B810189B, 2008.

Christoffersen, T. S., Hjorth, J., Horie, O., Jensen, N. R., Kotzias, D., Molander, L. L., Neeb, P., Ruppert, L., Winterhalter, R., Virkkula, A., Wirtz, K., and Larsen, B. R.: cis-

pinic acid, a possible precursor for organic aerosol formation from ozonolysis of α-pinene, Atmos. Environ., 32, 1657–1661, https://doi.org/10.1016/S1352-2310(97)00448-2, 1998.

Claeys, M., Szmigielski, R., Kourtchev, I., Van der Veken, P., Vermeylen, R., Maenhaut, W., Jaoui, M., Kleindienst, T. E., Lewandowski, M., Offenberg, J. H., and Edney, E. O.: Hydroxydicarboxylic Acids: Markers for Secondary Organic Aerosol from the Photooxidation of α-Pinene, Environ. Sci. Technol., 41, 1628–1634, https://doi.org/10.1021/es0620181, 2007.

Claeys, M., Iinuma, Y., Szmigielski, R., Surratt, J. D., Blockhuys, F., Van Alsenoy, C., Böge, O., Sierau, B., Gómez-González, Y., Vermeylen, R., Van der Veken, P., Shahgholi, M., Chan, A. W. H., Herrmann, H., Seinfeld, J. H., and Maenhaut, W.: Terpenylic Acid and Related Compounds from the Oxidation of α-Pinene: Implications for New Particle Formation and Growth above Forests, Environ. Sci. Technol., 43, 6976–6982, https://doi.org/10.1021/es9007596, 2009.

Dennington, R., Keith, T., and Millam, J.: Gauss View, Version 5, Semichem Inc., Shawnee Missio, 2009.

Feltracco, M., Barbaro, E., Contini, D., Zangrando, R., Toscano, G., Battistel, D., Barbante, C., and Gambaro, A.: Photo-oxidation products of α-pinene in coarse, fine and ultrafine aerosol: A new high sensitive HPLC-MS/MS method, Atmos. Environ., 180, 149–155, https://doi.org/10.1016/j.atmosenv.2018.02.052, 2018.

Finessi, E., Decesari, S., Paglione, M., Giulianelli, L., Carbone, C., Gilardoni, S., Fuzzi, S., Saarikoski, S., Raatikainen, T., Hillamo, R., Allan, J., Mentel, Th. F., Tiitta, P., Laaksonen, A., Petäjä, T., Kulmala, M., Worsnop, D. R., and Facchini, M. C.: Determination of the biogenic secondary organic aerosol fraction in the boreal forest by NMR spectroscopy, Atmos. Chem. Phys., 12, 941–959, https://doi.org/10.5194/acp-12-941-2012, 2012.

Frisch, M. J., Trucks, G. W., Schlegel, H. B., Scuseria, G. E., Robb, M. A., Cheeseman, J. R., Scalmani, G., Barone, V., Petersson, G. A., Nakatsuji, H., Li, X., Caricato, M., Marenich, A., Bloino, J., Janesko, B. G., Gomperts, R., Mennucci, B., Hratchian, H. P., Ortiz, J. V., Izmaylov, A. F., Sonnenberg, J. L., Williams-Young, D., Ding, F., Lipparini, F., Egidi, F., Goings, J., Peng, B., Petrone, A., Henderson, T., Ranasinghe, D., Zakrzewski, V. G., Gao, J., Rega, N., Zheng, G., Liang, W., Hada, M., Ehara, M., Toyota, K., Fukuda, R., Hasegawa, J., Ishida, M., Nakajima, T., Honda, Y., Kitao, O., Nakai, H., Vreven, T., Throssell, K., Montgomery Jr., J. A., Peralta, J. E., Ogliaro, F., Bearpark, M., Heyd, J. J., Brothers, E., Kudin, K. N., Staroverov, V. N., Keith, T., Kobayashi, R., Normand, J., Raghavachari, K., Rendell, A., Burant, J. C., Iyengar, S. S., Tomasi, J., Cossi, M., Millam, J. M., Klene, M., Adamo, C., Cammi, R., Ochterski, J. W., Martin, R. L., Morokuma, K., Farkas, O., Foresman, J. B., and Fox, D. J.: Gaussian 09, Revision A.02, Gaussian, Inc., Wallingford CT, 2016.

George, I. J. and Abbatt, J. P. D.: Chemical evolution of secondary organic aerosol from OH-initiated heterogeneous oxidation, Atmos. Chem. Phys., 10, 5551–5563, https://doi.org/10.5194/acp-10-5551-2010, 2010.

Glasius, M., Lahaniati, M., Calogirou, A., Di Bella, D., Jensen, N. R., Hjorth, J., Kotzias, D., and Larsen, B. R.: Carboxylic Acids in Secondary Aerosols from Oxidation of Cyclic Monoterpenes by Ozone, Environ. Sci. Technol., 34, 1001–1010, https://doi.org/10.1021/es990445r, 2000.

Goldstein, A. H. G., I. E.: Known and Unexplored Organic Constituents in the Earth's Atmosphere, Environ. Sci. Technol., 41, 1514–1521, https://doi.org/10.1021/es072476p, 2007.

Gómez-González, Y., Wang, W., Vermeylen, R., Chi, X., Neirynck, J., Janssens, I. A., Maenhaut, W., and Claeys, M.: Chemical characterisation of atmospheric aerosols during a 2007 summer field campaign at Brasschaat, Belgium: sources and source processes of biogenic secondary organic aerosol, Atmos. Chem. Phys., 12, 125–138, https://doi.org/10.5194/acp-12-125-2012, 2012.

Graedel, T.: Chemical Compounds in The Atmosphere, Elsevier Science, New York, USA, ISBN 9780124311862, 2012.

Hallquist, M., Wenger, J. C., Baltensperger, U., Rudich, Y., Simpson, D., Claeys, M., Dommen, J., Donahue, N. M., George, C., Goldstein, A. H., Hamilton, J. F., Herrmann, H., Hoffmann, T., Iinuma, Y., Jang, M., Jenkin, M. E., Jimenez, J. L., Kiendler-Scharr, A., Maenhaut, W., McFiggans, G., Mentel, Th. F., Monod, A., Prévôt, A. S. H., Seinfeld, J. H., Surratt, J. D., Szmigielski, R., and Wildt, J.: The formation, properties and impact of secondary organic aerosol: current and emerging issues, Atmos. Chem. Phys., 9, 5155–5236, https://doi.org/10.5194/acp-9-5155-2009, 2009.

Hirsikko, A., Nieminen, T., Gagné, S., Lehtipalo, K., Manninen, H. E., Ehn, M., Hõrrak, U., Kerminen, V.-M., Laakso, L., McMurry, P. H., Mirme, A., Mirme, S., Petäjä, T., Tammet, H., Vakkari, V., Vana, M., and Kulmala, M.: Atmospheric ions and nucleation: a review of observations, Atmos. Chem. Phys., 11, 767–798, https://doi.org/10.5194/acp-11-767-2011, 2011.

Hocart, C. H.: 9.10 – Mass Spectrometry: An Essential Tool for Trace Identification and Quantification, in: Comprehensive Natural Products II, edited by: Liu, H.-W. and Mander, L., Elsevier, Oxford, https://doi.org/10.1016/B978-008045382-8.00187-8, 327–388, 2010.

Hossaini, R., Chipperfield, M. P., Montzka, S. A., Leeson, A. A., Dhomse, S. S., and Pyle, J. A.: The increasing threat to stratospheric ozone from dichloromethane, Nat. Commun., 8, 15962, https://doi.org/10.1038/ncomms15962, 2017.

International Union of Pure and Applied Chemistry: mass-to-charge ratio, in: IUPAC Compendium of Chemical Terminology, 3rd edn., International Union of Pure and Applied Chemistry, version 3.0.1, https://doi.org/10.1351/goldbook.M03752, 2019.

Jarrold, C. C.: Probing Anion–Molecule Complexes of Atmospheric Relevance Using Anion Photoelectron Detachment Spectroscopy, ACS Physical Chemistry Au, 3, 17–29, https://doi.org/10.1021/acsphyschemau.2c00060, 2023.

Jenkin, E. M., Shallcross, D. E., and Harvey, J. N.: Development and application of a possible mechanism for the generation of cis-pinic acid from the ozonolysis of α- and β-pinene, Atmos. Environ., 34, 2837–2850, https://doi.org/10.1016/S1352-2310(00)00087-X, 2000.

Jia, Y., Tegtmeier, S., Atlas, E., and Quack, B.: How marine emissions of bromoform impact the remote atmosphere, Atmos. Chem. Phys., 19, 11089–11103, https://doi.org/10.5194/acp-19-11089-2019, 2019.

Kavouras, I. G., Mihalopoulos, N., and Stephanou, E. G.: Formation of atmospheric particles from organic acids produced by forests, Nature, 395, 683–686, https://doi.org/10.1038/27179, 1998.

Kavouras, I. G., Mihalopoulos, N., and Stephanou, E. G.: Secondary Organic Aerosol Formation vs Primary Organic Aerosol Emission: In Situ Evidence for the Chemical Coupling between

Monoterpene Acidic Photooxidation Products and New Particle Formation over Forests, Environ. Sci. Technol., 33, 1028–1037, https://doi.org/10.1021/es9807035, 1999.

Khalil, M. A. K. and Rasmussen, R. A.: Atmospheric chloroform, Atmos. Environ., 33, 1151–1158, https://doi.org/10.1016/S1352-2310(98)00233-7, 1999.

Kourtchev, I., Warnke, J., Maenhaut, W., Hoffmann, T., and Claeys, M.: Polar organic marker compounds in $PM_{2.5}$ aerosol from a mixed forest site in western Germany, Chemosphere, 73, 1308–1314, https://doi.org/10.1016/j.chemosphere.2008.07.011, 2008.

Krivácsy, Z., Molnár, Á., Tarjányi, E., Gelencsér, A., Kiss, G., and Hlavay, J.: Investigation of inorganic ions and organic acids in atmospheric aerosol by capillary electrophoresis, J. Chromatogr. A, 781, 223–231, https://doi.org/10.1016/S0021-9673(97)00290-2, 1997.

Li, L., Dai, D., Deng, S., Feng, J., Zhao, M., Wu, J., Liu, L., Yang, X., Wu, S., Qi, H., Yang, G., Zhang, X., Wang, Y., and Zhang, Y.: Concentration, distribution and variation of polar organic aerosol tracers in Ya'an, a middle-sized city in western China, Atmos. Res., 120–121, 29–42, https://doi.org/10.1016/j.atmosres.2012.07.024, 2013.

Lignell, H., Epstein, S. A., Marvin, M. R., Shemesh, D., Gerber, B., and Nizkorodov, S.: Experimental and Theoretical Study of Aqueous cis-Pinonic Acid Photolysis, J. Phys. Chem. A, 117, 12930–12945, https://doi.org/10.1021/jp4093018, 2013.

Ma, Y., Luciani, T., Porter, R. A., Russell, A. T., Johnson, D., and Marston, G.: Organic acid formation in the gas-phase ozonolysis of α-pinene, Phys. Chem. Chem. Phys., 9, 5084–5087, https://doi.org/10.1039/B709880D, 2007.

Ma, Y., Russell, A. T., and Marston, G.: Mechanisms for the formation of secondary organic aerosol components from the gas-phase ozonolysis of α-pinene, Phys. Chem. Chem. Phys., 10, 4294–4312, https://doi.org/10.1039/B803283A, 2008.

McAlister, A. B., Vesto, J. I., Huang, A., Wright, K. A., McLaughlin Sta. Maria, E. J., Bailey, G. M., Kretekos, N. P., Baldwin, P. R., Carrasquillo, A. J., and LaLonde, R. L.: Reactivity of a Carene-Derived Hydroxynitrate in Mixed Organic/Aqueous Matrices: Applying Synthetic Chemistry to Product Identification and Mechanistic Implications, Atmosphere, 12, 1617, https://doi.org/10.3390/atmos12121617, 2021.

McCrumb, J. L. and Arnold, F.: High-sensitivity detection of negative ions in the stratosphere, Nature, 294, 136–139, https://doi.org/10.1038/294136a0, 1981.

Miller, G. B. S., Esser, T. K., Knorke, H., Gewinner, S., Schöllkopf, W., Heine, N., Asmis, K. R., and Uggerud, E.: Spectroscopic Identification of a Bidentate Binding Motif in the Anionic Magnesium–CO_2 Complex ([ClMgCO2]-), Angew. Chem. Int. Ed., 53, 14407–14410, https://doi.org/10.1002/anie.201409444, 2014.

Moglioni, A. G., García-Expósito, E., Aguado, G. P., Parella, T., Branchadell, V., Moltrasio, G. Y., and Ortuño, R. M.: Divergent Routes to Chiral Cyclobutane Synthons from (-)-α-Pinene and Their Use in the Stereoselective Synthesis of Dehydro Amino Acids, J. Org. Chem., 65, 3934–3940, https://doi.org/10.1021/jo991773c, 2000.

Nozière, B., Kalberer, M., Claeys, M., Allan, J., D'Anna, B., Decesari, S., Finessi, E., Glasius, M., Grgić, I., Hamilton, J. F., Hoffmann, T., Iinuma, Y., Jaoui, M., Kahnt, A., Kampf, C. J., Kourtchev, I., Maenhaut, W., Marsden, N., Saarikoski, S., Schnelle-Kreis, J., Surratt, J. D., Szidat, S., Szmigielski, R., and Wisthaler, A.: The Molecular Identification of Organic Compounds in the Atmosphere: State of the Art and Challenges, Chem. Rev., 115, 3919–3983, https://doi.org/10.1021/cr5003485, 2015.

Olsson, P. Q. and Benner, R. L.: Atmospheric Chemistry and Physics: From Air Pollution to Climate Change By John H. Seinfeld (California Institute of Technology) and Spyros N. Pandis (Carnegie Mellon University). Wiley-VCH: New York. 1997. $89.95. xxvii + 1326 pp. ISBN 0-471-17815-2, J. Am. Chem. Soc., 121, 1423–1423, https://doi.org/10.1021/ja985605y, 1999.

Peeters, J., Vereecken, L., and Fantechi, G.: The detailed mechanism of the OH-initiated atmospheric oxidation of α-pinene: a theoretical study, Phys. Chem. Chem. Phys., 3, 5489–5504, https://doi.org/10.1039/B106555F, 2001.

Resch, J., Wolfer, K., Barth, A., and Kalberer, M.: Effects of storage conditions on the molecular-level composition of organic aerosol particles, Atmos. Chem. Phys., 23, 9161–9171, https://doi.org/10.5194/acp-23-9161-2023, 2023.

Richards, D. S., Trobaugh, K. L., Hajek-Herrera, J., Price, C. L., Sheldon, C. S., Davies, J. F., and Davis, R. D.: Ion-molecule interactions enable unexpected phase transitions in organic-inorganic aerosol, Science Advances, 6, eabb5643, https://doi.org/10.1126/sciadv.abb5643, 2020.

Rodriguez, A. A., Rafla, M. A., Welsh, H. G., Pennington, E. A., Casar, J. R., Hawkins, L. N., Jimenez, N. G., De Loera, A., Stewart, D. R., Rojas, A., Tran, M. K., Lin, P., Laskin, A., Formenti, P., Cazaunau, M., Pangui, E., Doussin, J. F., and De Haan, D. O.: Kinetics, Products, and Brown Carbon Formation by Aqueous-Phase Reactions of Glycolaldehyde with Atmospheric Amines and Ammonium Sulfate, J. Phys. Chem. A, 126, 5375–5385, https://doi.org/10.1021/acs.jpca.2c02606, 2022.

Ruff, D. J.: The Semi-Volatile Fraction of Atmospheric Aerosols, Thesis, Rochester Institute of Technology, https://repository.rit.edu/theses/9965 (last access: 12 August 2024), 2018.

Sarang, K., Otto, T., Gagan, S., Rudzinski, K., Schaefer, T., Brüggemann, M., Grgić, I., Kubas, A., Herrmann, H., and Szmigielski, R.: Aqueous-phase photo-oxidation of selected green leaf volatiles initiated by OH radicals: Products and atmospheric implications, Sci. Total Environ., 879, 162622, https://doi.org/10.1016/j.scitotenv.2023.162622, 2023.

Seinfeld, J. H. and Pandis, S. N.: Atmospheric chemistry and physics: from air pollution to climate change, John Wiley & Sons, ISBN 978-1-118-94740-1, 2016.

Shao, Y., Voliotis, A., Du, M., Wang, Y., Pereira, K., Hamilton, J., Alfarra, M. R., and McFiggans, G.: Chemical composition of secondary organic aerosol particles formed from mixtures of anthropogenic and biogenic precursors, Atmos. Chem. Phys., 22, 9799–9826, https://doi.org/10.5194/acp-22-9799-2022, 2022.

Szmigielski, R., Surratt, J. D., Gómez-González, Y., Van der Veken, P., Kourtchev, I., Vermeylen, R., Blockhuys, F., Jaoui, M., Kleindienst, T. E., Lewandowski, M., Offenberg, J. H., Edney, E. O., Seinfeld, J. H., Maenhaut, W., and Claeys, M.: 3-methyl-1,2,3-butanetricarboxylic acid: An atmospheric tracer for terpene secondary organic aerosol, Geophys. Res. Lett., 34, L24811, https://doi.org/10.1029/2007GL031338, 2007.

Tajuelo, M., Rodriguez, A., Aranda, A., Díaz-de-Mera, Y., Tucceri, M. E., and Rodriguez, D.: Secondary organic aerosol formation from photooxidation of γ-butyro and γ-valero-lactone: A com-

bined experimental and theoretical study, Atmos. Environ., 276, 119051, https://doi.org/10.1016/j.atmosenv.2022.119051, 2022.

Takahama, S., Ruggeri, G., and Dillner, A. M.: Analysis of functional groups in atmospheric aerosols by infrared spectroscopy: sparse methods for statistical selection of relevant absorption bands, Atmos. Meas. Tech., 9, 3429–3454, https://doi.org/10.5194/amt-9-3429-2016, 2016.

van den Berg, F.: Measured and computed concentrations of methyl isothiocyanate in the air around fumigated fields, Atmos. Environ. A-Gen., 27, 63–71, https://doi.org/10.1016/0960-1686(93)90071-6, 1993.

Van Den Berg, F., Roos, A. H., Tuinstra, L. G. M. T., and Leistra, M.: Measured and computed concentrations of 1,3-dichloropropene and methyl isothiocyanate in air in a region with intensive use of soil fumigants, Water Air Soil Poll., 78, 247–264, https://doi.org/10.1007/BF00483035, 1994.

Watts, S. F.: The mass budgets of carbonyl sulfide, dimethyl sulfide, carbon disulfide and hydrogen sulfide, Atmos. Environ., 34, 761–779, https://doi.org/10.1016/S1352-2310(99)00342-8, 2000.

Winterhalter, R., Van Dingenen, R., Larsen, B. R., Jensen, N. R., and Hjorth, J.: LC-MS analysis of aerosol particles from the oxidation of α-pinene by ozone and OH-radicals, Atmos. Chem. Phys. Discuss., 2003, 1–39, https://doi.org/10.5194/acpd-3-1-2003, 2003.

Yasmeen, F., Vermeylen, R., Szmigielski, R., Iinuma, Y., Böge, O., Herrmann, H., Maenhaut, W., and Claeys, M.: Terpenylic acid and related compounds: precursors for dimers in secondary organic aerosol from the ozonolysis of α- and β-pinene, Atmos. Chem. Phys., 10, 9383–9392, https://doi.org/10.5194/acp-10-9383-2010, 2010.

Yu, Z., Jang, M., Zhang, T., Madhu, A., and Han, S.: Simulation of Monoterpene SOA Formation by Multiphase Reactions Using Explicit Mechanisms, ACS Earth and Space Chemistry, 5, 1455–1467, https://doi.org/10.1021/acsearthspacechem.1c00056, 2021.

Zanca, N., Lambe, A. T., Massoli, P., Paglione, M., Croasdale, D. R., Parmar, Y., Tagliavini, E., Gilardoni, S., and Decesari, S.: Characterizing source fingerprints and ageing processes in laboratory-generated secondary organic aerosols using proton-nuclear magnetic resonance (^{1}H-NMR) analysis and HPLC HULIS determination, Atmos. Chem. Phys., 17, 10405–10421, https://doi.org/10.5194/acp-17-10405-2017, 2017.

Zhang, X., McVay, R. C., Huang, D. D., Dalleska, N. F., Aumont, B., Flagan, R. C., and Seinfeld, J. H.: Formation and evolution of molecular products in α-pinene secondary organic aerosol, P. Natl. Acad. Sci. USA, 112, 14168–14173, 2015.